Carbon 109 (2016) 666–672

Contents lists available at ScienceDirect

Carbon

journal homepage: www.elsevier.com/locate/carbon

The microscopic deformation mechanism of 3D graphene foam materials under uniaxial compression

Chao Wang [a], Cun Zhang [b], Shaohua Chen [c, *]

[a] LNM, Institute of Mechanics, Chinese Academy of Sciences, Beijing, 100190, China
[b] Department of Engineering Mechanics, Shijiazhuang Tiedao University, Shijiazhuang, 050043, China
[c] Institute of Advanced Structure Technology, Beijing Institute of Technology, Beijing, 100081, China

ARTICLE INFO

Article history:
Received 23 April 2016
Received in revised form
15 August 2016
Accepted 27 August 2016
Available online 30 August 2016

ABSTRACT

Recent experiments have shown that the graphene foam material exhibits a rubber-like constitutive behavior and a near-zero Poisson's ratio. We have performed coarse grain molecular dynamics simulations, which show that these intriguing phenomena can be attributed to the microstructure deformation, rearrangement and compaction in three stages, respectively. The elastic deformation of microstructures leads to the initial linear behavior of the graphene foam material. Microstructure rearrangement, including bending, self-folding and flake-rotation, should be responsible for the second stage with a good performance of deformation but with a low bearing capacity. Microstructure compaction leads to a high bearing capacity at the last stage. A near-zero Poisson's ratio of the material within a certain range of compressive strain is also found to be due to the microstructure rearrangement, which induces soft flakes to fill the empty space without volume expansion in the other directions. Furthermore, it demonstrates that Poisson's ratio of such a type of material can be further tuned by the stiffness of graphene flakes as well as the amplitude of external strain. This study highlights the promise of graphene foam materials for energy absorption and dissipation under extreme conditions.

1. Introduction

Graphene is a typically two-dimensional sheet composed of single-layer carbon atoms, which possesses a large specific surface area, extraordinary mechanical [1], thermal [2] and electrical [3] properties. It has been widely used in recent years as exceptional nanoscale building blocks to assemble a large number of new materials [4–16]. Among them, the graphene foam material [5–7], as a porous nano-material composed of different-layer flakes, has received much attention from engineers and material scientists due to its incredible high porosity of 99% and intrinsic potential as an ideal scaffold. It can be modulated by introducing functional additives or chemical groups into the pore-rich structure to achieve required properties. A series of novel properties have been reported, including super-elasticity [6], good electrical conductivity [17], high efficient energy absorption [18], excellent electrochemical stability [19], which enable wide promising applications in sensing [20], lithium ion batteries [21], sorbent materials [22], stretchable electronics [17], and so on.

To understand the underlying deformation mechanism of graphene foam materials and disclose the structure-property relationship is of vital importance for optimal design of novel multifunctional materials and applications in a broad field. Both regular platelets and long graphene ribbons of different-layer graphene flakes [5] are used to assemble graphene foam materials. Various structures, such as biomimetic honeycomb-like [23], multiple nano-ball [19], hierarchical pores [24] etc., are designed to construct material frameworks. Lots of work has been carried out on graphene foam materials [6,7,17,23,24] to characterize component flakes, analyze structural characteristics and measure some physical and mechanical properties. Uniaxial compression experiments were adopted in most of these works to find the stress-strain response, where a rubber-like compressive constitutive relationship was always obtained for such a new foam-material. Specially, a near-zero Poisson's ratio was observed by Wu et al. [6] in their as-synthesized graphene foam materials. Multi-scale deformation mechanism of a 3D graphene foam material was carried out by Nieto et al. [5] with in situ SEM, in which the micro-structural evolution with graphene flake rotating to align in the tensile

* Corresponding author.
E-mail address: chenshaohua72@hotmail.com (S. Chen).

http://dx.doi.org/10.1016/j.carbon.2016.08.084
0008-6223/

direction was observed. In addition, graphene flake bending and cell-wall elastic depression were found to be two main deformation mechanisms in nano-indentation experiments [5]. With a full-atom molecular dynamics simulation technique, Baimova et al. [25] investigated the mechanical response of graphene foam materials subjected to shear strain and found that the shear deformation could alter the microstructure and mechanical properties of the graphene foam material. However, many questions are still open with regard to such a novel material, whose mechanical properties is totally different from those of a single graphene and graphite [26–28]. What kind of microscopic deformation mechanism in graphene foam materials induces a rubber-like constitutive relation? How to explain the near-zero Poisson's ratio of a graphene foam material? Is the Poisson's ratio of a graphene foam material always near-zero or influenced by any factor? Answering the above questions should be very useful for further design of advanced graphene foam materials.

In the present paper, the technique of coarse-grained molecular dynamics simulation (CGMD) is adopted, which is advantageous in contrast to the time-consuming full-atom molecular dynamics method and the inconvenient in-site experimental observation. Furthermore, the CGMD method has been well verified to successfully study many graphene-related problems, such as the mechanical property of a single- or multi-layer graphene [29,30], adsorption of surfactants [31], self-assembly and penetration of graphene sheets in membranes [32,33], etc..

The outline of this paper is as follows. Section 2 introduces the simulation model of a graphene foam material under uniaxial compression as well as the methodology of this paper. The constitutive relation of graphene-foam materials and the microscopic deformation mechanism are investigated in Section 3. The near-zero Poisson's ratio observed in recent experiments will be discussed in Section 4, where the microscopic mechanism affecting the Poisson's ratio of such a novel material will be disclosed as well as some other influencing factors. Conclusions will be given finally.

2. Model and methodology

The coarse-grained model of a graphene sheet developed by Cranford et al. [30] is well adopted in this paper, which is based on the equivalent energy principle between a full-atom simulation and a twisted graphene ribbon. A two-dimensional graphene sheet is simulated by a square grid, in which each coarse grain represents a 25 Å × 25 Å atomic graphene sheet. A harmonic spring potential $\phi_T = k_T(r-r_0)^2/2$ is used to describe the axial stretching energy among all pairs of bonded particles, where k_T denotes a spring constant and r is the distance between two particles with an equilibrium distance $r_0 = 25$ Å. A harmonic rotational-spring potential $\phi_\varphi = k_\varphi(\varphi-\varphi_0)^2/2$ is used to describe the in-plane bending energy under shear deformation, where k_φ denotes the spring constant related to the bending angle φ among three particles with an equilibrium angle $\varphi_0 = 90^\circ$. $\phi_\theta = k_\theta(\theta\text{-}\theta_0)^2/2$ denotes the out-of-plane bending energy with a spring constant k_θ, where θ denotes the bending angle among three particles with an equilibrium value $\theta_0 = 180^\circ$. The weak van der Waals interaction between neighboring coarse-grained flakes is defined as a Lennard-Jones potential $\phi_{LJ} = 4\varepsilon((\sigma/r)^{12}\text{-}(\sigma/r)^6)$, where ε is a parameter determining the depth of the potential well, σ is a length scale parameter that determines the position of the minimum potential, and r is the atom-to-atom distance. According to [30], σ and ε are set as 23.84 Å and 473 kcal/mol in this paper, respectively. As a building block, the side length of each square coarse-grained flake is 25 nm, which contains one hundred beads as shown in Fig. 1a. As for the pre-processing of a graphene foam system, all flakes are placed randomly in a big cubic box to ensure no interaction among them. Then, NPT assemble technique is adopted to deal with the system with a periodic boundary condition in three directions as well as a constant temperature 300 K and one barometric pressure. As a result, the system would shrink gradually and finally reach an equilibrium state at about 30 ns with a time step 1fs. Then, the ambient pressure is reset to zero. Under the berendsen barostat 0 Pa and Langevin thermostat 300 K, the system would expand slightly and reach the final equilibrium state at about 500 ns with the criterion that the total energy fluctuation converges to less than 1%. The final configuration is shown in Fig. 1b, in which the flakes are randomly oriented. Periodic boundary conditions are adopted in three directions in order to simulate a bulk material. For simplicity, all flakes in a simulation material are assumed to be identical. Materials composed of flakes of different layers are considered in this paper in order to investigate the effect of stiffness of flakes on the mechanical behavior and give insights into the design of novel graphene foam materials. One should be noted that sliding between neighboring layers in a single flake is not involved with an assumption that the interface between adjacent layers is strong enough to resist interface sliding. Such a strong interface between graphene layers can be realized by chemical treatment, such as moderate electron-beam irradiation inside a transmission electron microscope [34], or adding some chemical groups between layers [35]. The real thickness (layer number) of flakes in real materials is in the range of one to ten graphene layers [5,17,36]. In our simulation, the flake consists of one-, two-, four- and eight-layer graphene sheets, respectively. According to [30] and [37], both the tensile stiffness and the in-plane bending stiffness increase linearly with the flake thickness, while the out-of-plane bending stiffness will increase nearly proportional to cubic of the flake thickness. With regard to the flake of different layers, the corresponding coarse-grained parameters k_T, k_φ and k_θ are given in Table 1, which can be tuned simultaneously for a typical graphene foam material.

The equilibrium density of graphene foam in a series of experimental studies [6,17,23,36] is in the range of 1–100 mg/cm^3. During the simulation, we find that the equilibrium density of the graphene foam decreases with an increasing flake size. For example, when the size of a square flake increases from 25 to 125 nm, the equilibrium density of the graphene foam material decreases from 475 to 72 mg/cm^3. The size of each flake reported in experiments varies from several nanometers [38] to micrometers [6]. A relatively small size 25 nm is chosen in our numerical calculation due to two reasons: (a) No matter how large the flake is, four kinds of contact microstructures are found to be basic ones. We tried to establish foam structures with flakes of different sizes and found that only the porosity or density is different; (b) The computation complexity would increase sharply if relatively large flakes are chosen, even with CGMD technique.

Within an equilibrium simulation system, four kinds of microstructures are found as shown Fig. 1(c)-1(f), which include different links between point-surface, edge-edge, surface-surface and edge-surface. Here, one should be noted that the “point” here denotes essentially a small part of a flake. In addition, more than two flakes may be in contact and contact microstructures in the material system, we focus mainly on the smallest composed microstructure to study the interaction micro-mechanism. The distribution proportion of four kinds of contact microstructures in the system composed of 8-layer flakes is counted, where the amount is 10.27%, 35.62%, 4.79%, 49.32% for point-surface, edge-edge, surface-surface and edge-surface contact microstructures, respectively. It is further found that the edge-edge and edge-surface contact microstructures are two main ones in graphene foam materials no mater the flake is stiff or soft (thick or thin). The four kinds of microstructures have already been well identified in SEM experimental observations [6,24,39], but the distribution proportion was not counted

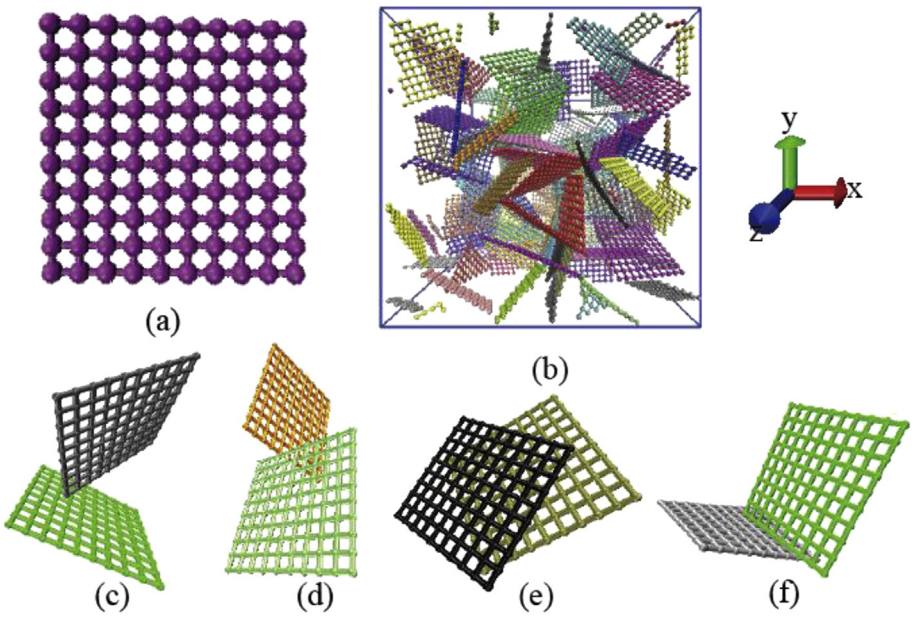

Fig. 1. Schematic of the simulation model and microstructures. (a) Flake composed of coarse-grained graphene. (b) The initial configuration of an equilibrated coarse-grained graphene foam material. (c–f) Four kinds of contact microstructures: point-surface, edge-edge, surface-surface and edge-surface. The mechanical property of all flakes is identical in a material. (A colour version of this figure can be viewed online.)

Table 1
Spring constants in different potential energy functions adopted to describe different mechanical behaviors of coarse-grained graphene sheets [30].

Parameters	No. of graphene layers				Units
	1	2	4	8	
k_T	470	930	1860	3720	kcal mol^{-1}Å^{-2}
k_φ	16870	33740	67480	134960	kcal mol^{-1}rad^{-2}
k_θ	144.9	8970	82731	933087	kcal mol^{-1}rad^{-2}

experimentally. As a primary investigation of graphene foam materials with CGMD technique, the effect of geometry and morphology of flakes, density of materials as well as some possible physical or chemical additives are not included in this paper.

If no otherwise specified, uniaxial compression acted in the x-direction with a loading velocity 1 m/s corresponding to a strain rate 10^7 s^{-1} is adopted in the simulation without any pressure in the other two directions. All the simulations are implemented with an open source software Large-scale Atomic/Molecular Massively Parallel Simulator (LAMMPS) [40].

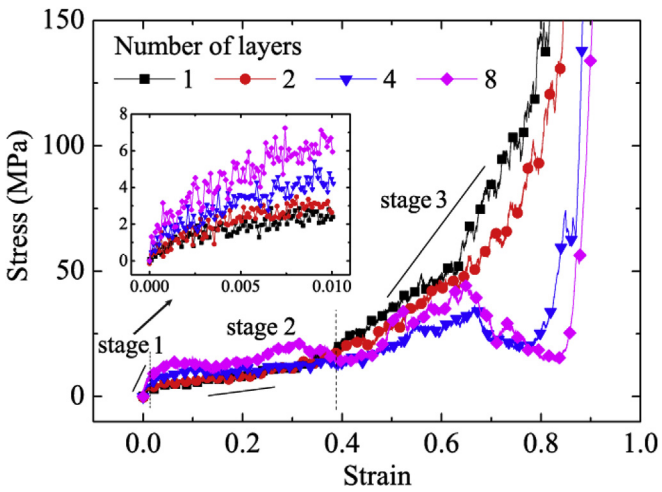

Fig. 2. The uniaxially compressive stress-strain relation of graphene foam materials composed of flakes of different layers. The inset is the amplification of the curves in stage 1. (A colour version of this figure can be viewed online.)

3. Compressive stress-strain relation

A typical rubber-like stress-strain response has been measured experimentally for graphene foam materials under uniaxial compression [6,7,36]. However, what is the microscopic deformation mechanism of such a special material behavior? A series of simulations are carried out on the model shown in Fig. 1(b) with uniaxial compressive loading in the x-direction. The compressive stress-strain relations of four kinds of systems composed of flakes of different thickness are achieved numerically as shown in Fig. 2. Similar to the rubber-like stress-strain response found in uniaxial compression experiments [6,7,36], the typical constitutive relation consists of three stages.

When the strain is smaller than 0.01, the graphene foam material is elastic and there is no flake rearrangement or obvious microstructural evolution occurring during stage 1. Details can be found in Fig. S1 in Supplementary materials. At stage 2, the strain increases sharply to about 0.4 but with a slightly increasing stress. Both the strain and the stress increase obviously at stage 3 when the compressive strain is larger than 0.4. Comparing the stress-strain curves of four kinds of systems yields that the elastic modulus of the system increases with an increasing stiffness of component flakes at stage 1; Similarly, at stage 2, the stress in the material with relatively stiff flakes is also relatively large. However, the situation is on the contrary at the last stage. Furthermore, one may note that a significant drop in the stress-strain curve emerges for the graphene foam material with relatively thick flakes at the last stage. It should be due to the rearrangement among stiff flakes with joint breaking, bodily rotating or separation perpendicular to the compressive strain direction in order to release the over-bending energy in stiff flakes. All the phenomena could be

observed in movies in Supplementary Materials. The basic characteristic in the rubber-like stress-strain relation obtained by our simulations is comparable to the experimental result qualitatively. However, it is hardly possible to compare with the experimental result quantitatively due to many un-given information in experiments, for example, the flake size, shape, thickness, porosity etc. The stress-strain cycles with load and release processes are further simulated for such a foam material and given in Fig. S2 in Supplementary materials, which is also comparable to the existing experimental results [6,24,39] and can be used to analyze the characteristic of energy dissipation of such a foam material in our future work.

Three typical snapshots for two kinds of graphene foam materials are recorded, respectively, where one kind of material is composed of relatively stiff flakes and the other one consists of relatively soft flakes. The snapshots are shown in Fig. 3, where Fig. 3(a)-(c) denote the stiff one and Fig. 3(d)-(f) denote the soft one. In both cases, each snapshot represents each deformation stage of the constitutive relation. Both the two kinds of graphene foam materials experience a small elastic deformation without rearrangement of microstructures as shown in both Fig. 3(a) and (d), respectively. As a result, a linear elastic behavior is exhibited at the stage 1 under a small compressive strain. By contrast, all the flakes in both materials rearrange themselves obviously under a relative large compressive strain, which leads to an only slightly increasing stress but a good ability of deformation, corresponding to the stage 2 in the constitutive relation curve. Finally, after the uttermost rearrangement of microstructures, the graphene foam material is compacted as shown in Fig. 3(c) and (f), which has an excellent loading bearing capacity, but a poor ability of deformation, corresponding to the constitutive curves in stage 3.

In order to get to the bottom of the deformation mechanism, evolution of the four kinds of microstructures is checked in two typical graphene foam materials under different strain, i.e., materials composed of 1-layer flakes and 8-layer flakes, respectively. Variation of each kind of microstructure along with an increasing compressive strain can be found clearly as shown in Fig. 4 for three kinds of strain states 0, 0.4 and 0.8. Microscopic rearrangement of component flakes can be easily identified from the four groups, including in-plane and out-of-plane rotation, in-plane and out-of-plane bending and buckling, self-folding, sliding and separation. As a result, all the microstructures are finally compacted in the direction of the external compressive loading.

It is much easy to understand all the phenomena if we imagine the graphene foam material as a block composed of papers. No matter what the stiffness of the paper, the block can sustain a compressive stress only if the compressive strain is small enough, which corresponds to the initially linear elastic stage of a graphene foam material. The larger the stiffness of the paper, the larger the whole stiffness of the block will be at the initial stage. Along with the increase of the external compressive strain, each paper or paper bundle in the block will rearrange themselves in the form of rotating, bending or buckling, self-folding or sliding, similar to the second stage in the graphene foam material. The block will be compacted under a large compressive strain, in which the density of the block composed by soft papers should be larger than the counterpart with stiff papers, analogous to the last stage in a graphene foam material. With this in mind, it is convenient to understand the stress-strain relation and the deformation mechanism for a graphene foam material from the microscopic point of view. As for the sudden drop in the stress-strain relation of graphene foam materials composed of stiff flakes under large compressive strain, it should be due to the rearrangement among stiff flakes with joint breaking, bodily rotating or separation perpendicular to the compressive strain direction as shown in Fig. 4(c), (i), 4(o) and 4(u), in order to release the over-bending energy in stiff flakes.

Further study on the effect of loading rates on the mechanical behavior and microstructure evolution is simply carried out. The stress-strain relations of graphene foam materials under different strain rates are analyzed. It is clear that the whole variation trend of

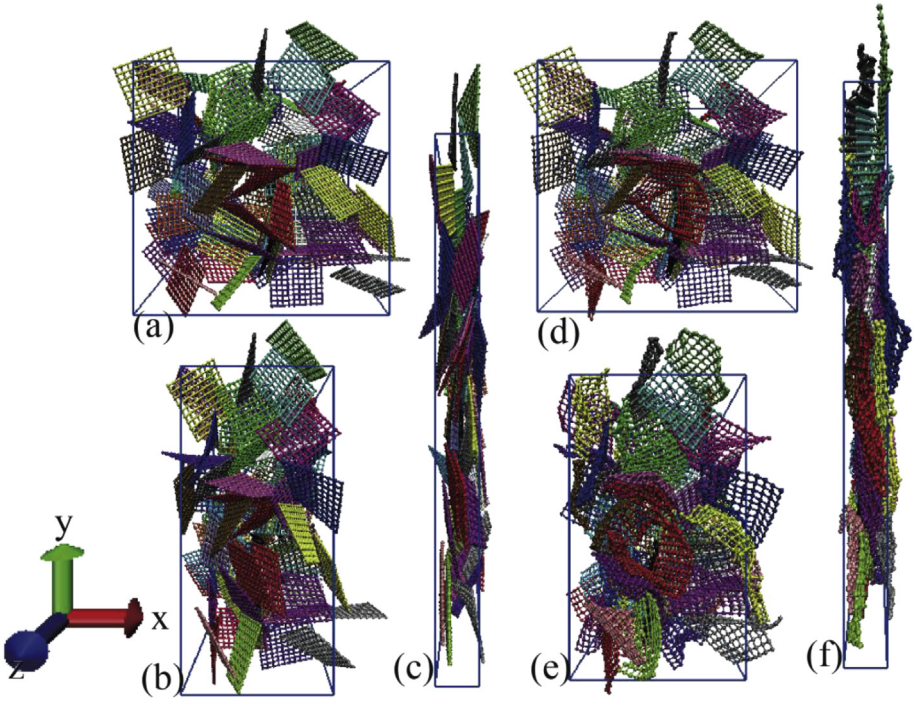

Fig. 3. Snapshots of the deformed simulation model at the strain of 0, 0.4 and 0.8, respectively. (a–c) For the graphene foam material composed of 8-layer flakes. (d–f) For the graphene foam material composed of 1-layer flakes. (A colour version of this figure can be viewed online.)

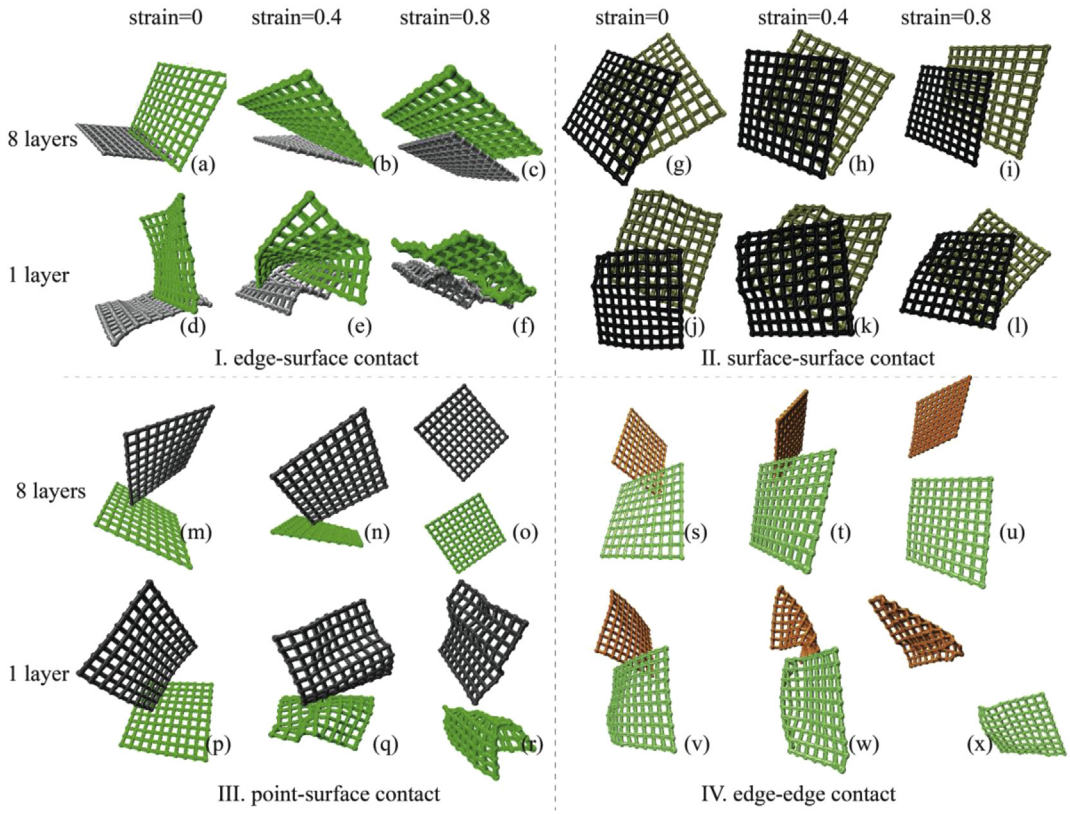

Fig. 4. Snapshots of the four basic microstructures at the compressive strain of 0, 0.4 and 0.8 for graphene foam materials composed of 1-layer flakes and 8-layer flakes. (A colour version of this figure can be viewed online.)

the constitutive relation is not affected by the strain rate, except for the initial stiffness at stage 1 and the value of the stress at stage 2 and stage 3. Both the initial stiffness and the bearing capacity improve with an increasing strain rate, leading to a rubber-like rate-dependent material as shown in Fig. 5. Numerical observation further shows that the microscopic deformation mechanism is insensitive to the strain rate, but the evolution rate of microstructures is significantly affected by the loading rate. Three movies are provided in Supplementary materials to show the microstructural evolution for an identical system, but under different compressive strain rates 10^8, 10^7 and 10^6 s^{-1}. Details are omitted here for simplicity.

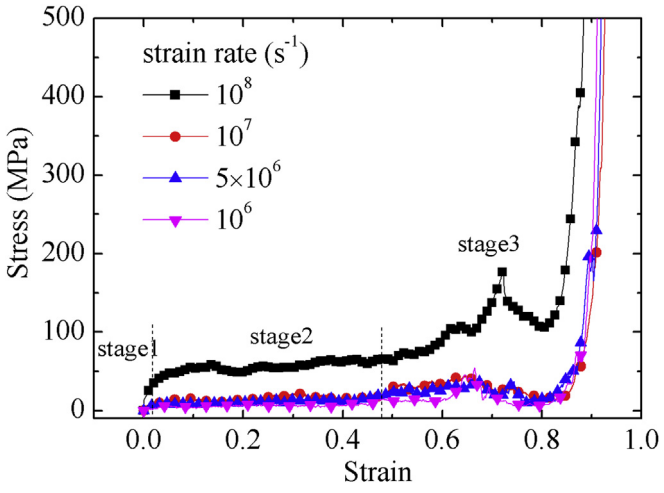

Fig. 5. The stress-strain relations of graphene foam materials under compression of different strain rates. (A colour version of this figure can be viewed online.)

Supplementary video related to this article can be found at http://dx.doi.org/10.1016/j.carbon.2016.08.084.

4. Poisson's ratio of graphene foam materials

The Poisson's ratio in both y-axis and z-axis directions as a function of the compressive strain in the x-axis direction is studied in this section for graphene foam materials composed of 1-layer flake. It is found that both relations coincide with each other as shown in Fig. 6(a), demonstrating an isotropic feature of such a material. Along with an increasing compressive strain, the Poisson's ratio reduces from an initially small positive value to a near-zero even a negative one, then increases again. Considering the stiffness effect of flakes, the Poisson's ratio as a function of the compressive strain is shown in Fig. 6(b) for materials composed of different-layer flakes. It is found that the Poisson's ratio is significantly influenced by the stiffness of flakes in the material. The Poisson's ratio in all cases undergoes a "U"-type variation, though the falling is very weak for materials composed of relatively stiff flakes as shown in Fig. 6(b). Furthermore, under a fixed compressive strain, the stiffer the flake, the larger the Poisson's ratio of the material will be. Effects of the compressive strain and the mechanical properties of flakes on Poisson's ratio of the foam material are directly shown in Fig. S3 in Supplementary materials. Such a result is different and should be very interesting in contrast to the classical conception of a constant Poisson's ratio for ordinary materials.

The microstructure evolution in such materials should be concerned again, which should be responsible for the variation

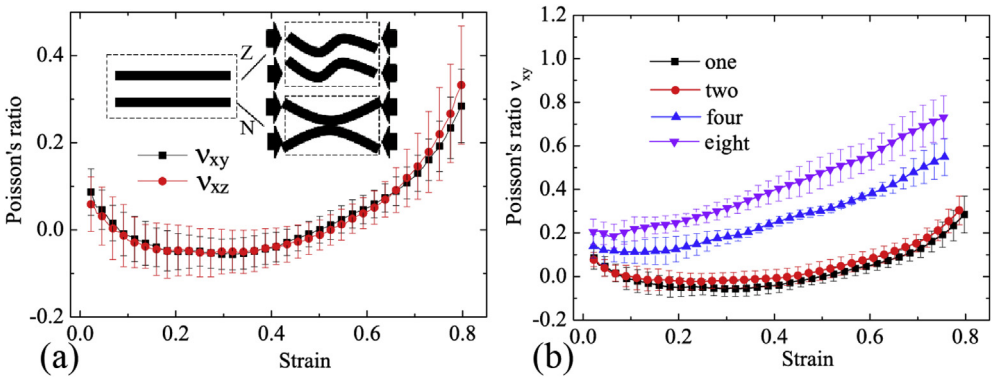

Fig. 6. Poisson's ratio of the graphene foam material as a function of the compressive strain. (a) Poisson's ratios ν_{xy} and ν_{xz} for the graphene foam material composed of 1-layer flakes. (b) Poisson's ratio ν_{xy} for the graphene foam material composed of flakes of different layers. (A colour version of this figure can be viewed online.)

mechanism of Poisson's ratios. Corresponding to the initially small loading, no matter what the stiffness of the flakes is, elastic deformation of the flakes should happen. As a result, a positive Poisson's ratio is achieved. Along with an increasing external loading, either in the material composed of soft flakes or in the material composed of stiff flakes, rearrangement of microstructures will happen. For graphene foam materials composed of soft flakes, the flexible sheet may bend or self-fold in the compressive direction, which leads to the space around them occupied without volume expansion. During the process, two possible micro-mechanisms may dominate as shown in the inset of Fig. 6a, a "Z"-type deformation and a "N"-type one. If flakes bend or self-fold randomly, a near-zero Poisson's ratio should be yielded. Such a case is labeled as a "Z"-type. However, if more flakes tend to bend inwards as shown by the inset labeled as a "N"-type in Fig. 6(a), shrinkage perpendicular to the loading direction would happen, leading to a negative Poisson's ratio. Such a microscopic mechanism is also applicable to some other materials, such as cell structure materials [41] and carbon nanotube films [42]. When the material is compressed by a relative large strain, the microstructure becomes compact in the loading direction. Behaviors of bending, self-folding, rotating will induce inflation perpendicular to the loading direction, leading to an increasing Poisson's ratio. In contrast to the graphene foam materials composed of soft flakes, self-folding seldom happens in the material with stiff flakes. Expanding perpendicular to the compressive loading direction rather than filling the empty space dominates, which yields the "only little-drop" feature of Poisson's ratio for materials composed of stiff flakes as shown in Fig. 6(b).

One should be noted that the value of Poisson's ratio of such a graphene foam has some discrete features as shown in Fig. 6(a) and (b). It is also influenced by the material density and the external loading rate, the details of which can be found in Figs. S4 and S5 in Supplementary materials.

All the above analysis shows that Poisson's ratio of graphene foam materials could be tuned in a wide range from negative to positive in real applications.

5. Conclusions

Coarse-grained molecular dynamic simulations are carried out in this paper in order to investigate the mechanical properties of 3D graphene foam materials from the microscopic point of view and disclose the corresponding microstructure deformation mechanism. The rubber-like constitutive behavior of such a material under a uniaxial compressive loading is achieved, which consists of three typical stages. Simulation results exhibit that the first linear stage in the constitutive relation is attributed to the elastic deformation of microstructures no matter what the stiffness of microstructures is. The second stage corresponds to a good ability of deformation but a poor bearing capacity, which is mainly because of the microstructure rearrangement, including flake bending, self-folding as well as rotation in the empty space. When the external compressive strain is large enough, the inside microstructure is compacted, leading to a high bearing capacity at the last stage. With regard to the Poisson's ratio of graphene foam materials composed of flakes of different stiffness, a "U"-type variation trend is commonly found along with increasing compressive strain, which depends significantly on the microstructure deformation mechanism too. A near-zero Poisson's ratio could be achieved in graphene foam materials composed of relative soft flakes, for example, a single-layer coarse-grained graphene. Both the stiffness of flakes and the amplitude of external strain will show significant influence on the Poisson's ratio, which demonstrates that the Poisson's ratio of graphene foam materials could be tuned effectively in a wide range. These results are significant for understanding the deformation mechanism of materials composed of graphene sheets and the design of graphene foam materials with special functions, for example, energy absorption and dissipation.

Acknowledgements

The work reported here is supported by NSFC through Grants #11532013, #11372317, #11502150 and the 973 Nano-project (2012CB937500).

Appendix A. Supplementary data

Supplementary data related to this article can be found at http://dx.doi.org/10.1016/j.carbon.2016.08.084.

References

[1] W. Wei, X. Qu, Extraordinary physical properties of functionalized graphene, Small 8 (2012) 2138–2151.
[2] A.A. Balandin, S. Ghosh, W. Bao, I. Calizo, D. Teweldebrhan, F. Miao, et al., Superior thermal conductivity of single-layer graphene, Nano Lett. 8 (2008) 902–907.
[3] C.N.R. Rao, A.K. Sood, R. Voggu, K.S. Subrahmanyam, Some novel attributes of graphene, J. Phys. Chem. Lett. 1 (2010) 572–580.
[4] L. Zhang, N.T. Alvarez, M. Zhang, M. Haase, R. Malik, D. Mast, et al., Preparation and characterization of graphene paper for electromagnetic interference shielding, Carbon 82 (2015) 353–359.
[5] A. Nieto, B. Boesl, A. Agarwal, Multi-scale intrinsic deformation mechanisms of 3D graphene foam, Carbon 85 (2015) 299–308.
[6] Y. Wu, N. Yi, L. Huang, T. Zhang, S. Fang, H. Chang, et al., Three-dimensionally bonded spongy graphene material with super compressive elasticity and

near-zero Poisson's ratio, Nat. Commun. 6 (2015) 6141.
[7] Q. Peng, Y. Li, X. He, X. Gui, Y. Shang, C. Wang, et al., Graphene nanoribbon aerogels unzipped from carbon nanotube sponges, Adv. Mater. 26 (2014) 3241–3247.
[8] F. Meng, W. Lu, Q. Li, J.-H. Byun, Y. Oh, T.-W. Chou, Graphene-based fibers: a review, Adv. Mater. 27 (2015) 5113–5131.
[9] Z. Xu, H. Sun, X. Zhao, C. Gao, Ultrastrong fibers assembled from giant graphene oxide sheets, Adv. Mater. 25 (2013) 188–193.
[10] S.M. Yoon, W.M. Choi, H. Baik, H.J. Shin, I. Song, M.S. Kwon, et al., Synthesis of multilayer graphene balls by carbon segregation from nickel nanoparticles, ACS Nano 6 (2012) 6803–6811.
[11] H. Wang, L. Shi, T. Yan, J. Zhang, Q. Zhong, D. Zhang, Design of graphene-coated hollow mesoporous carbon spheres as high performance electrodes for capacitive deionization, J. Mater. Chem. A 2 (2014) 4739–4750.
[12] H. Chen, S. Chen, The fracture behaviors of carbon nanotube and nanoscroll reinforced silicon matrix composites, Carbon 67 (2014) 344–351.
[13] W. Zhang, H. Xie, R. Zhang, M. Jian, C. Wang, Q. Zheng, et al., Synthesis of three-dimensional carbon nanotube/graphene hybrid materials by a two-step chemical vapor deposition process, Carbon 86 (2015) 358–362.
[14] Y. Zhu, L. Li, C. Zhang, G. Casillas, Z. Sun, Z. Yan, et al., A seamless three-dimensional carbon nanotube graphene hybrid material, Nat. Commun. 3 (2012) 1–7.
[15] S. Stankovich, Dikin Da, G.H.B. Dommett, K.M. Kohlhaas, E.J. Zimney, Stach Ea, et al., Graphene-based composite materials, Nature 442 (2006) 282–286.
[16] Q. Zhang, X. Xu, H. Li, G. Xiong, H. Hu, T.S. Fisher, Mechanically robust honeycomb graphene aerogel multifunctional polymer composites, Carbon 93 (2015) 659–670.
[17] Z. Chen, W. Ren, L. Gao, B. Liu, S. Pei, H.-M. Cheng, Three-dimensional flexible and conductive interconnected graphene networks grown by chemical vapour deposition, Nat. Mater. 10 (2011) 424–428.
[18] Y. Ma, H. Chang, M. Zhang, Y. Chen, Graphene-based materials for lithium-ion hybrid supercapacitors, Adv. Mater. 27 (2015) 5296–5308.
[19] Q. Shao, J. Tang, Y. Lin, F. Zhang, J. Yuan, H. Zhang, et al., Synthesis and characterization of graphene hollow spheres for application in supercapacitors, J. Mater. Chem. A 1 (2013) 15423–15428.
[20] F. Yavari, Z. Chen, A.V. Thomas, W. Ren, H.-M. Cheng, N. Koratkar, High sensitivity gas detection using a macroscopic three-dimensional graphene foam network, Sci. Rep. 1 (2011) 1–5.
[21] S. Chen, P. Bao, X. Huang, B. Sun, G. Wang, Hierarchical 3D mesoporous silicon@graphene nanoarchitectures for lithium ion batteries with superior performance, Nano Res. 7 (2014) 85–94.
[22] H. Bi, X. Xie, K. Yin, Y. Zhou, S. Wan, L. He, et al., Spongy graphene as a highly efficient and recyclable sorbent for oils and organic solvents, Adv. Funct. Mater. 22 (2012) 4421–4425.
[23] L. Qiu, J.Z. Liu, S.L.Y. Chang, Y. Wu, D. Li, Biomimetic superelastic graphene-based cellular monoliths, Nat. Commun. 3 (2012) 1–7.
[24] R. Zhang, Y. Cao, P. Li, X. Zang, P. Sun, K. Wang, et al., Three-dimensional porous graphene sponges assembled with the combination of surfactant and freeze-drying, Nano Res. 7 (2014) 1477–1487.
[25] Baimova Ja, L.K. Rysaeva, B. Liu, S.V. Dmitriev, K. Zhou, From flat graphene to bulk carbon nanostructures, Phys. Status Solidi B Basic Solid State Phys. 252 (2015) 1502–1507.
[26] A. Politano, G. Chiarello, Probing the Young's modulus and Poisson's ratio in graphene/metal interfaces and graphite: a comparative study, Nano Res. 8 (6) (2015) 1847–1856.
[27] J.-L. Tsai, J.-F. Tu, Characterizing mechanical properties of graphite using molecular dynamics simulation, Mater. Des. 31 (1) (2010) 194–199.
[28] H. Zhao, K. Min, N. Aluru, Size and chirality dependent elastic properties of graphene nanoribbons under uniaxial tension, Nano Lett. 9 (8) (2009) 3012–3015.
[29] L. Ruiz, W. Xia, Z. Meng, S. Keten, A coarse-grained model for the mechanical behavior of multi-layer graphene, Carbon 82 (2015) 103–115.
[30] S. Cranford, M.J. Buehler, Twisted and coiled ultralong multilayer graphene ribbons, Model Simul. Mater. Sci. Eng. 19 (2011) 054003.
[31] D. Wu, X. Yang, Coarse-grained molecular simulation of self-assembly for nonionic surfactants on graphene nanostructures, J. Phys. Chem. B 116 (2012) 12048–12056.
[32] A.V. Titov, P. Kral, R. Pearson, Sandwiched Graphene–Membrane superstructures, ACS Nano 4 (2010) 229–234.
[33] J. Wang, Y. Wei, X. Shi, H. Gao, Cellular entry of graphene nanosheets: the role of thickness, oxidation and surface adsorption, RSC Adv. 3 (2013) 15776.
[34] A. Kis, G. Csányi, J.-P. Salvetat, T.-N. Lee, E. Couteau, A.J. Kulik, et al., Reinforcement of single-walled carbon nanotube bundles by intertube bridging, Nat. Mater. 3 (2004) 153–157.
[35] Q. Cheng, M. Li, L. Jiang, Z. Tang, Bioinspired layered composites based on flattened double-walled carbon nanotubes, Adv. Mater. 24 (14) (2012) 1838–1843.
[36] H. Bi, I.-W. Chen, T. Lin, F. Huang, A new tubular graphene form of a tetrahedrally connected cellular structure, Adv. Mater. 27 (2015) 5943–5949.
[37] L.J. Gibson, M.F. Ashby, Cellular Solids: Structure and Properties, Cambridge University Press, 1999.
[38] W. Deng, Q. Fang, X. Zhou, H. Cao, Z. Liu, Hydrothermal self-assembly of graphene foams with controllable pore size, RSC Adv. 6 (2016) 20843–20849.
[39] H. Hu, Z. Zhao, W. Wan, Y. Gogotsi, J. Qiu, Ultralight and highly compressible graphene aerogels, Adv. Mater. 25 (2013) 2219–2223.
[40] S. Plimpton, Fast Parallel algorithms for short-range molecular dynamics, J. Comput. Phys. 117 (1) (1995) 1–19.
[41] R. Lakes, Foam structures with a negative Poisson's ratio, Science 235 (4792) (1987) 1038–1040.
[42] Y.J. Ma, X.F. Yao, Q.S. Zheng, Y.J. Yin, D.J. Jiang, G.H. Xu, et al., Carbon nanotube films change Poisson's ratios from negative to positive, Appl. Phys. Lett. 97 (2010) 3–5.